

Full-scale testing on the flexural behavior of an innovative dovetail UHPC joint of composite bridges

Jianan Qi*, Zhao Cheng^a, Jingquan Wang^b, Yutong Zhu^c and Wenchao Li^d

Key Laboratory of Concrete and Prestressed Concrete Structures of the Ministry of Education, School of Civil Engineering, Southeast University, Nanjing, China

(Received June 4, 2019, Revised January 31, 2020, Accepted February 10, 2020)

Abstract. This paper presents a full-scale experimental test to investigate the flexural behavior of an innovative dovetail ultra-high performance concrete (UHPC) joint designed for the 5th Nanjing Yangtze River Bridge. The test specimen had a dimension of 3600 × 1600 × 170 mm, in accordance with the real bridge. The failure mode, crack pattern and structural response were presented. The ductility and stiffness degradation of the tested specimens were explicitly discussed. Test results indicated that different from conventional reinforced concrete slabs, well-distributed cracks with small spacing were observed for UHPC joint slabs at failure. The average nominal flexural cracking strength of the test specimens was 7.7 MPa, signifying good crack resistance of the proposed dovetail UHPC joint. It is recommended that high grade reinforcement be cooperatively used to take full advantage of the superior mechanical property of UHPC. A new ductility index, expressed by dividing the ultimate deflection by flexural cracking deflection, was introduced to evaluate the post-cracking ductility capacity. Finally, a strut-and-tie (STM) model was developed to predict the ultimate strength of the proposed UHPC joint.

Keywords: composite bridge; ultra-high performance concrete (UHPC); joint; flexural behavior; STM model

1. Introduction

Ultra-high performance concrete (UHPC) is a cementitious-based composite material with superior mechanical properties and excellent durability (Le Hoang and Fehling 2017a, Le Hoang and Fehling 2017b, Qi *et al.* 2017, Nguyen *et al.* 2019). Randomly dispersed steel fibers significantly improve the material properties and thus resulting in high performance structures (Saleem *et al.* 2011, Saleem *et al.* 2012, Pourbaba *et al.* 2018, Mirmiran *et al.* 2019, Pourbaba *et al.* 2019, Qi *et al.* 2019a). Over the past few decades, numerous bridges with UHPC components have been constructed all over the world, including steel-UHPC composite bridges, prestressed UHPC box girder bridges and UHPC pedestrian bridges, etc. (Graybeal 2008, Russell *et al.* 2013, Zhou *et al.* 2018, Farzad *et al.* 2019, Wang *et al.* 2019). In a recent application, precast UHPC deck was utilized over the open steel box girder in the 5th Nanjing Yangtze River Bridge as it offers better fatigue cracking resistance than steel bridge deck.

The 5th Nanjing Yangtze River Bridge in Nanjing, China is a three-tower, cable-stayed bridge with a total length of 1796 m, consisting of two main spans at 600 m, two side spans at 218 m and two extension spans at 80 m (Fig. 1(a)). The open steel box girder with composite precast UHPC deck is adopted for the main span due to excellent torsion resistance. Because of the superior mechanical properties of UHPC, the thickness of the UHPC deck slab is reduced to 2/3 of that for normal strength concrete deck, thereby significantly decreasing the self-weight of the bridge deck. As shown in Fig. 1(b), the width and height of the composite girder are 35.6 m and 3.6 m, respectively, in which a standard segmental unit (blue dash line) of the bridge girder has a longitudinal length of 14.6 m. The bridge deck units are manufactured in factory and then assembled through cast-in-place joints (green part) in field. The slab of a deck unit includes four precast UHPC slabs (gray part). Each slab is connected to the steel box girder by welding the embedded steel plates to the girder diaphragms (Fig. 1b). After completing the precast panel installation, the cast-in-factory deck slab (orange part) is poured. An innovative dovetail UHPC joint was developed to improve the joint mechanical behavior between precast panels and the cast-in-factory deck slab. Under wheel loads and other repetitive loads, the fatigue cracks may develop in such joints. Therefore, their cracking resistance and strength need to be evaluated.

Numerous efforts have been made to investigate the cracking resistance of the UHPC joints. Haber and Graybeal (2018) conducted an experimental test investigating on the flexural behavior of different UHPC-class materials connecting prefabricated bridge elements (PBE) using noncontact lap splices. The dimensions of the test

*Corresponding author, Ph.D., Assistant Professor

E-mail: qjianan723@126.com

^a Postdoctoral Fellow

E-mail: zcheng@seu.edu.cn

^b Ph.D., Professor

E-mail: wangjingquan@seu.edu.cn

^c Master student

E-mail: 434771650@qq.com

^d Graduate Student

E-mail: 519064452@qq.com

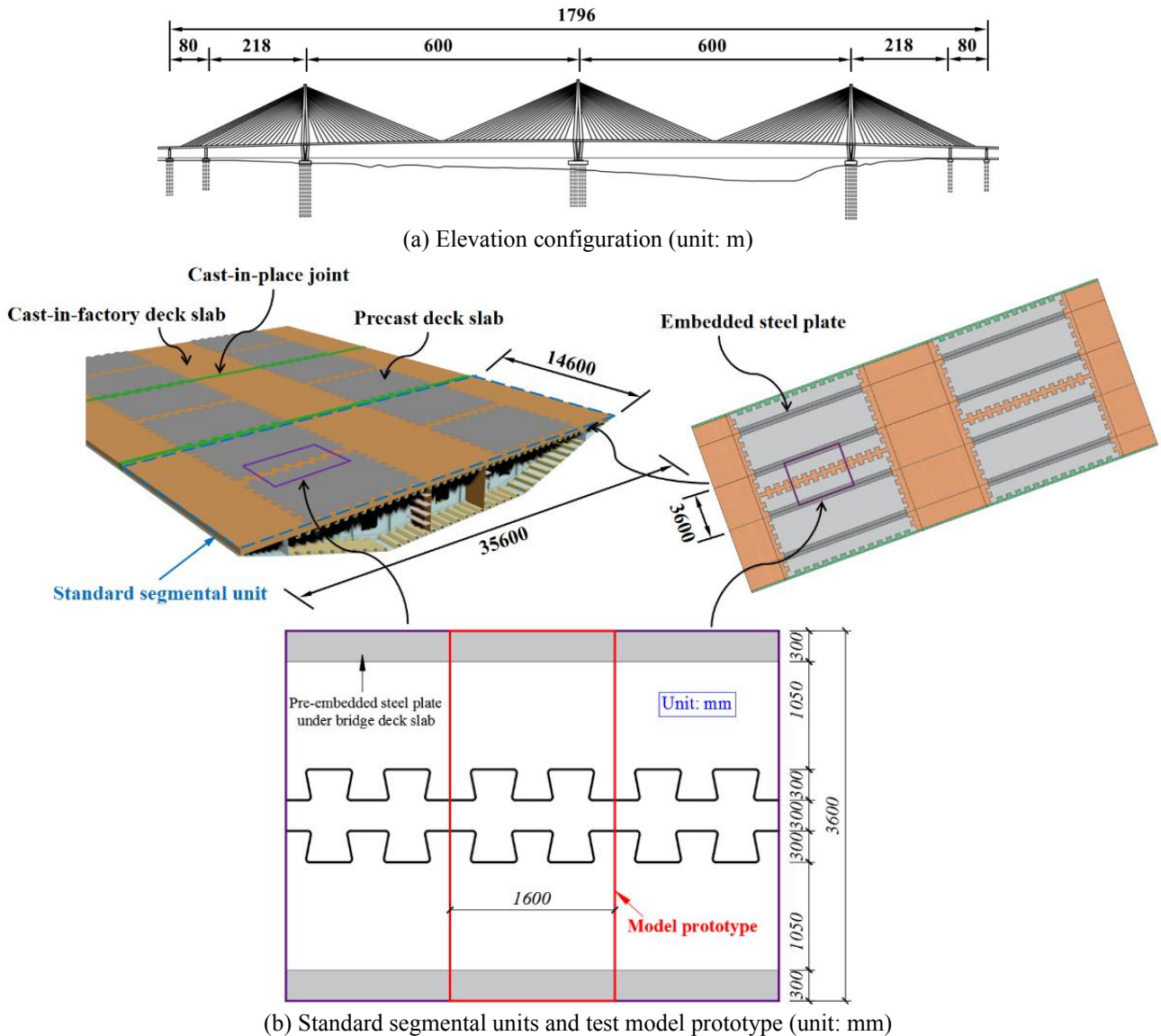


Fig. 1 The 5th Nanjing Yangtze River Bridge and test model prototype

specimens were $2286 \times 711 \times 152$ mm. They found that the UHPC-connection region exhibited good performance and little damage. De la Varga *et al.* (2018) proposed a set of potential strategies using UHPC as joint material to enhance the shrinkage properties and bond performance of prefabricated bridge deck connection grouts using the same size specimens. Verger-Leboeuf *et al.* (2017) pointed out that transverse UHPC field-cast connections do not modify the failure mode, ultimate strength and stiffness of a slab differently than the equivalent cast-in-place systems via an experimental study on seven $3000 \times 1200 \times 200$ mm specimens. Arafa *et al.* (2016) experimentally investigated the behavior of UHPC joints between precast normal concrete panels using nine $3000 \times 1000 \times 225$ mm specimens and demonstrated that joints showed sufficient strength and performance and the failure occurred in the spliced concrete panels. Lee and Lee (2015) pointed out that a minimum joint width of 150 mm could satisfy the anchorage requirement based on the test on fourteen $3000 \times 780 \times 220$

mm specimens. Grace *et al.* (2012) demonstrated that the UHPC connections using straight, noncontact lap-spliced bars were sufficient for creating monolithic action between the adjacent decked T-girders. Graybeal (2010) experimentally investigated the high cycle fatigue and static behavior of PBEs connected by UHPC joints on six $2400 \times 2152 \times 200$ mm specimens. He pointed out that the straight bar noncontact lap-splice details were sufficient to resist service and ultimate loads. It can be concluded that most existing research focused on the reduced scale model experiment and limited comparative information can be found in terms of the structural behavior of full-scale UHPC joint bridge deck slabs.

This paper presents an experimental investigation examining the flexural behavior of the innovative dovetail UHPC joint developed for the 5th Nanjing Yangtze River Bridge. The testing specimens reproduced the full-scaled dovetail UHPC joint and were subjected to four-point bending test. The crack pattern and failure mode are

presented. The flexural behavior, ductility, and stiffness degradation of the tested specimens are explicitly discussed. In addition, a strut-and-tie model to predict the joint strength is proposed.

2. Experimental investigation

2.1 Mixture proportions and material properties

A new UHPC mix was developed for this study. Fig. 2 shows the mixture proportion and material mechanical property of the new developed UHPC. Due to its ready availability, the fine river sand with maximum grain size of 5 mm and fineness modulus of 2.6 was used. Conventional UHPC typically has a relatively low modulus of elasticity due to the lack of hard coarse aggregate. To improve the modulus of elasticity, the UHPC developed for this study contained coarse aggregate with a size ranging from 5 mm to 8 mm. A high-active admixture SBT®-HDC was added for improving the mechanical performance and viscosity of the UHPC. This admixture had a density of 2.56 g/cm³, a specific surface area of 1230 m²/kg, and an activity index at 28 days of 115%. Considering steel fibers as a part of longitudinal reinforcement (Bandelt and Billington 2016, Parra-Montesinos 2005), a fiber volume fraction of 2% was adopted for the UHPC in this study.

As indicated in our previous studies, the mixing procedure of the developed UHPC was carefully selected and executed due to its unique characteristics (Qi *et al.* 2018a, Qi *et al.* 2018b, Qi *et al.* 2019b, Qi *et al.* 2019c). Cementitious material and aggregate were firstly mixed for 5 min, followed by adding water and additives to stir for 5 min. Steel fibers were then uniformly added into the mixture followed by a 5 min final mixing. The material property of the developed UHPC is shown in Fig. 2. The compressive strength, f_{cu} was obtained from uniaxial compression tests on three 150 × 150 × 150 mm cubic specimens, and the tensile strength, f_t were established from uniaxial tension tests on three 100 × 50 mm dog-bone specimens. The modulus of elasticity, E_c was determined from three 100 × 100 × 300 mm prism specimens according to the Chinese Code (GB/T 50081-2002 2002).

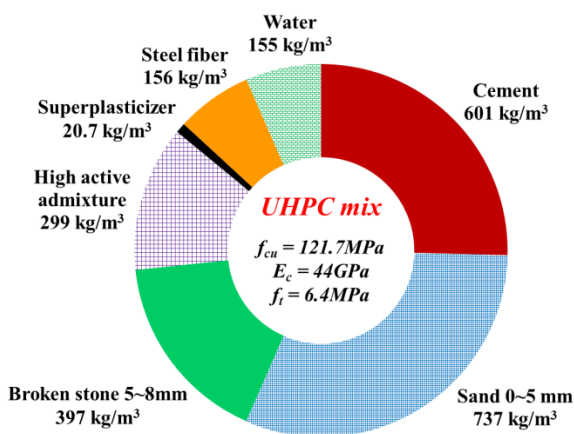


Fig. 2 UHPC mix and properties

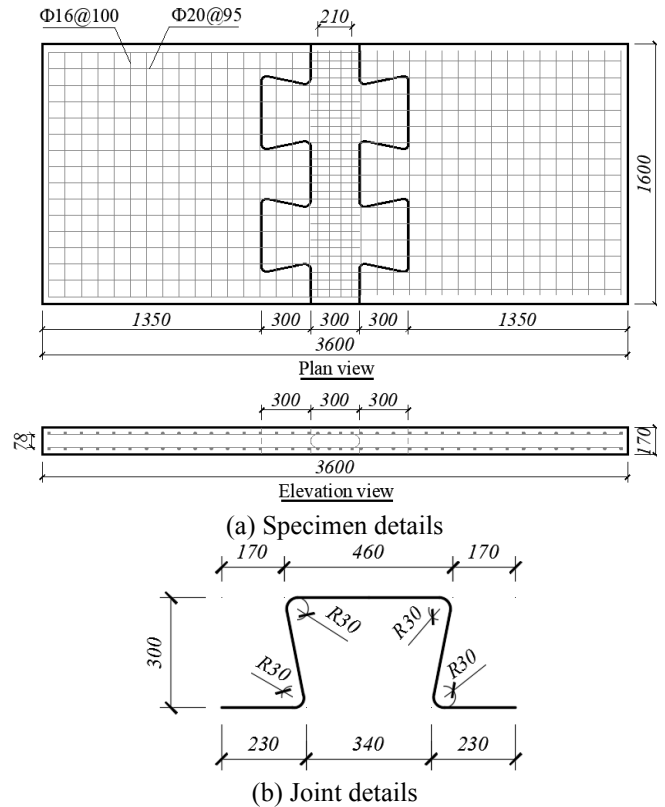


Fig. 3 Dimensions of specimens (unit: mm)

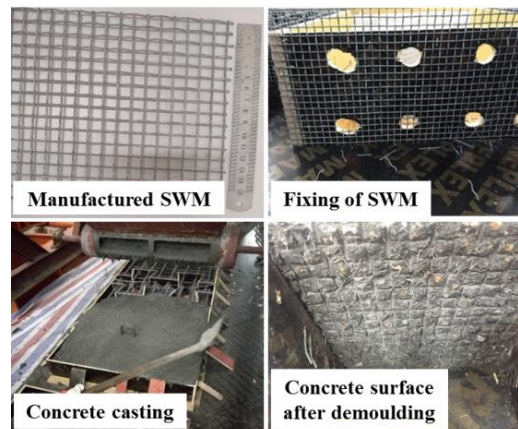


Fig. 4 A new interfacial treatment by steel wire mesh

2.2 Specimen design

Three identical specimens, as show in Fig. 3, were fabricated to represent the full-scaled dovetail joint in the deck of the 5th Nanjing Yangtze River Bridge. Fig. 3(a) shows the dimensions and reinforcement details of the test specimens. The length and width of the slab were 3600 mm and 1600 mm, respectively. A deck thickness of 170 mm was selected to keep in accordance with that of the bridge deck. Two types of reinforcements with diameters of 20 mm and 16 mm were used as longitudinal reinforcement and transversal reinforcement. The yield strength and ultimate tensile strength of the longitudinal reinforcement were 460.1 MPa and 616.0 MPa, respectively, and the yield strength and ultimate tensile strength of the transversal

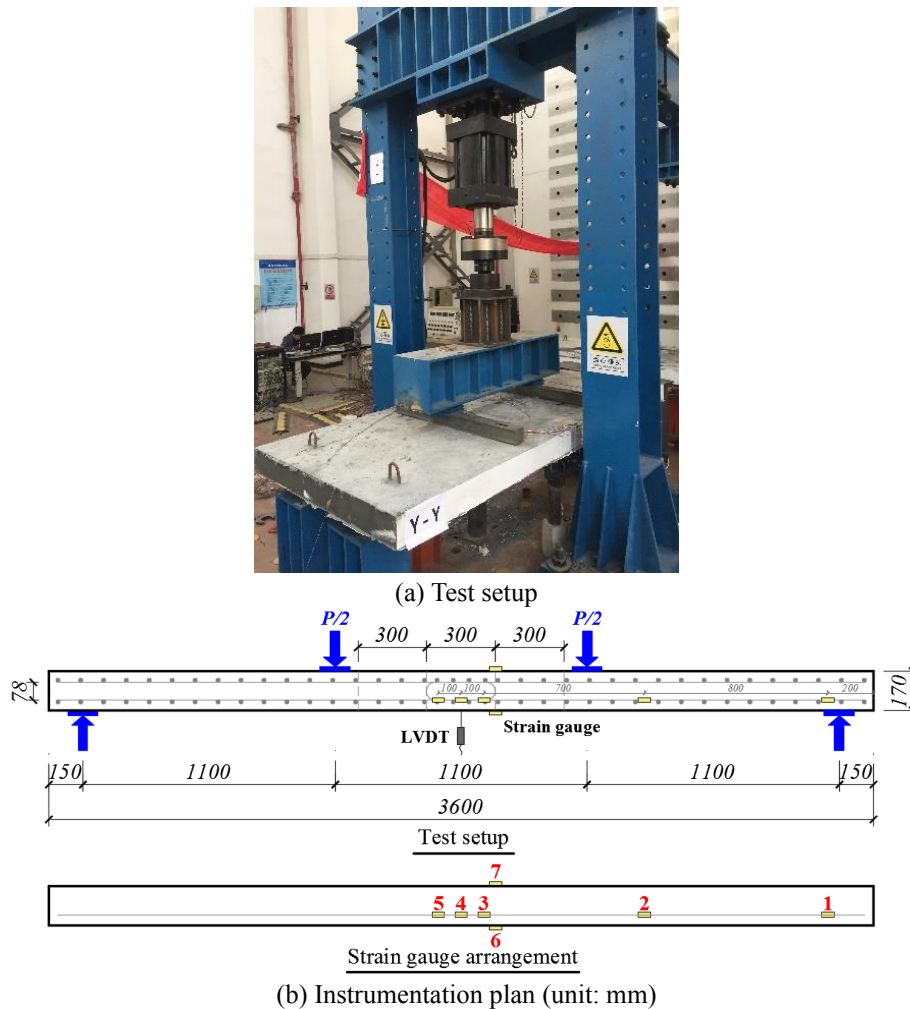


Fig. 5 Test setup and instrumentation plan

reinforcement were 526.0 MPa and 667.0 MPa, respectively. The joint was made in an innovative dovetail shape in order to improve the joint mechanical performance. Fig. 3(b) shows the details of the dovetail joint. U-bars with a bend angle of 180° were used with the aim of improving the mechanical anchorage performance.

A specimen consisted of two precast slab components, which were connected by a cast-in-place middle dovetail joint for simulating the real construction process. A new interface treating technology, named as steel wire mesh (SWM) method, was proposed here to enhance the interfacial bond property. Fig. 4 illustrates the manufacturing process of the proposed SWM method. Wires with a diameter of 3 mm were woven into a 10 mm by 10 mm wire mesh and then the SWM was attached in the side face of the formwork before casting concrete. After hardening of the concrete mass, the SWM was removed from the precast slab. It can be seen that numerous steel fibers were exposed after removing the SWM. Therefore, the SWM method did not only significantly create the surface roughness but also provided an additional fiber bridging mechanism between the cast-in-place joint and the precast slabs. After casting the concrete, specimens were covered with plastic sheeting and were cured under laboratory conditions prior to the removal of the formwork.

Prior to testing, the tension surface of the specimen was grinded to smooth and painted white to facilitate visual inspection for the identification of any cracking.

2.3 Test setup and procedure

Fig. 5 shows the test setup and the instrumentation plan. As shown in Fig. 5(a), the specimens were subjected to a four-point bending test, allowing the flexural behavior of the joint region to be examined with no shear present. The downward loads were applied in a monotonically increasing manner. Before testing, the specimen was loaded to 10 kN and then maintained stable for 5 minutes to ensure the working performance of instruments and then unloaded. During testing, the loading rate was set at 10 kN/minute before the first crack was observed, and then increased to 20 kN/minute until the strain of the longitudinal reinforcement at mid-span reached its yielding strength. Thereafter, the load was continuously increased at a rate of 10 kN/minute until failure. The specimen mid-span deflection was measured by a linear variable differential transformer (LVDT). In addition, the strains at longitudinal reinforcement and the top and bottom of the specimen were monitored using the strain gauges. The locations of gauges is presented in Fig. 5 (b).

Table 1 Summary of test results

| Specimen number | Flexural cracking | | | Yielding state | | Ultimate state | | Ductility index | | Failure mode |
|-----------------|-------------------|--------------------|---------------------|----------------|-----------------|----------------|-----------------|------------------------|---------------------|------------------------|
| | P_{cr} (kN) | Δ_{cr} (mm) | σ_{cr} (MPa) | P_y (kN) | Δ_y (mm) | P_u (kN) | Δ_u (mm) | Δ_u/Δ_{cr} | Δ_u/Δ_y | |
| F-1 | 111.8 | 3.1 | 8.0 | 630.9 | 60.8 | 707 | 125 | 40.3 | 2.1 | Flexure ^{a,b} |
| F-2 | 104.6 | 3.3 | 7.5 | 634.8 | 48.1 | 712 | 110 | 33.3 | 2.3 | Flexure ^{a,b} |
| F-3 | 108.2 | 3.2 | 7.7 | 631.2 | 44.1 | 715 | 97.8 | 30.6 | 2.2 | Flexure ^{a,b} |

Note: P_p = peak load; Δ_p = peak load deflection; P_{cr} = flexural cracking load; Δ_{cr} = flexural cracking deflection; σ_{cr} = nominal flexural cracking strength; P_y = longitudinal reinforcement yielding load; Δ_y = longitudinal reinforcement yielding deflection.

^a Yielding of longitudinal reinforcement.

^b Large expansion of flexural crack.

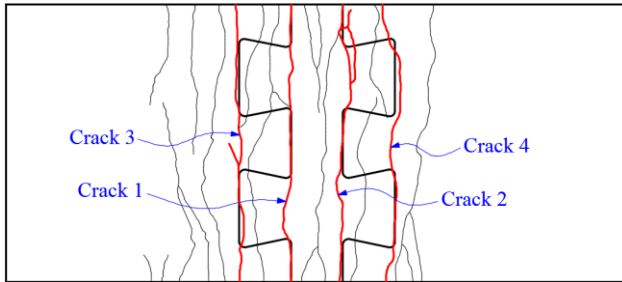
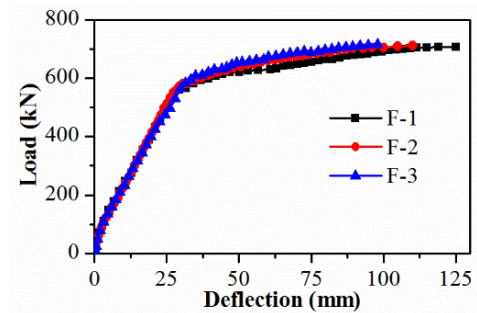


Fig. 6 Typical crack distribution at failure

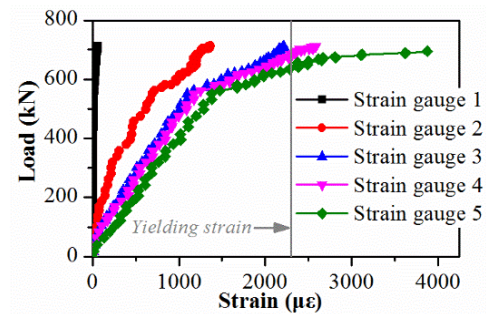
3. Test results and discussions

3.1 Failure mode and crack pattern

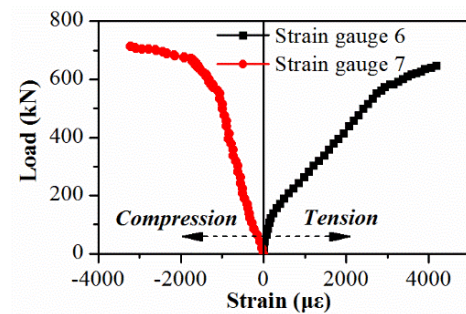
Table 1 summarizes the main quantitative information of each test specimen. The three identical specimens showed similar structural responses regarding flexural cracking strength, ultimate strength and crack propagation. All specimens experienced flexural failure along with longitudinal reinforcement yielding and large expansion of flexural cracks. The average nominal flexural cracking strength of the test specimens is 7.7 MPa (corresponding to a crack width of 0.05 mm), signifying good crack resistance of the proposed dovetail UHPC joint slabs. At failure, the ratio of deflection to span is about 1/30, indicating good deformability and ductility. Fig. 6 presents the typical crack distribution for the test specimens at the end of test. Two flexural cracks (crack 1 and crack 2) initially appeared at the joint inner side at a small applied load followed by the appearance of the flexural cracks (crack 3 and crack 4) at the joint outside as the load slightly increased. Multiple micro cracks subsequently occurred at the pure bending region, indicating that fiber bridging effect restrained the propagation of flexural cracks and facilitated multiple cracking on the tension region of the specimen. The existing crack propagated in the transversal direction of the slab and formed a whole transversal crack as the load increased. It is interesting to find that an audible sizzling sound was heard during the loading, which evidenced that the fibers were pulled out from the matrix. Once a crack appeared, fibers crossing the crack were pulled out from the matrix and were activated in resisting tension forces, which helped redistributing and homogenizing the concrete stress beside cracks. The fiber bridging effect allowed for more short fine cracks to develop adjacent to the existing cracks at small



(a) Load-deflection curves



(b) Load-longitudinal reinforcement strain curves



(c) Load-concrete strain curves

Fig. 7 Structural responses

spacing. After yielding of longitudinal reinforcement, the subsequent increasing of the load led to a continuous opening and height increasing of formerly existing cracks, which resulted in a continuous increment in slab deflection. Finally, flexural failure occurred for all specimens. Different from conventional reinforced concrete (RC) slabs, it is interesting to find that the compression zone concrete failed locally instead of extensively crushing at failure although the concrete compressive strain exceeded ultimate compressive strain.

3.2 Structural responses

Fig. 7 shows the structural responses, including load-deflection curves, load-longitudinal reinforcement strain curves and load-concrete strain curves of the test specimens. Note that the location of the strain gauges is illustrated in Fig. 5.

Load versus mid-span deflection curves - The three specimens showed similar load-deflection response, as shown in Fig. 7(a). The flexural response of the proposed dovetail UHPC joint slabs was explicitly divided into three stages: 1) linear elastic stage before flexural cracking; 2) the stage after cracking and prior to yielding of longitudinal reinforcement; and 3) the stage after longitudinal reinforcement yielding. A linear load-deflection response was obtained prior to flexural cracking and an approximately linear behavior with a slight reduction in specimen stiffness was detected after the appearance of visible flexural cracks on the test specimens. Then, the specimens showed obvious nonlinear behavior when the longitudinal reinforcement began to yield.

Load versus longitudinal reinforcement strain curves - The load versus longitudinal reinforcement strains at different sections is shown in Fig. 7(b). The reinforcement strain at the location 200 mm from the end of the longitudinal reinforcement was almost 0 during the whole loading process, indicating that the anchorage length of 20 mm reinforcement is larger than 200 mm. However, the longitudinal reinforcement strains at and near mid-span sections exceeded the yielding strain, indicating that the U type bars could satisfy the anchorage requirement.

Load versus concrete strain curves - Curves with the tension and compression sides' concrete surface strain at the dovetail joint section versus the applied load are plotted in Fig. 7(c). Positive strains indicate tensile strains of the bottom concrete surface while negative strains represent compressive strains of the top concrete surface. Both compressive and tensile strains stayed at a small value before flexural cracking. After the appearance of visible flexural cracks, the tensile strains of the bottom concrete surface increased dramatically and exceeded the ultimate tensile strain. Some strain gauges were fractured because of the excessive tensile strain. The compressive strain increased linearly and then non-linearly before and after the yielding of the longitudinal reinforcement.

3.3 Ductility

Ductility index can be used to quantitatively evaluate the ductility of RC structures with expressions of deflection, curvature, or rotational ductility. Deflection ductility index is broadly adopted by most researchers because of its simplicity of expression (Qi *et al.* 2016, Yoo and Yoon 2015). The following two expressions of deflection ductility index are usually used

$$\mu_p = \frac{\Delta_p}{\Delta_y} \quad (1a)$$

$$\mu_u = \frac{\Delta_u}{\Delta_y} \quad (1b)$$

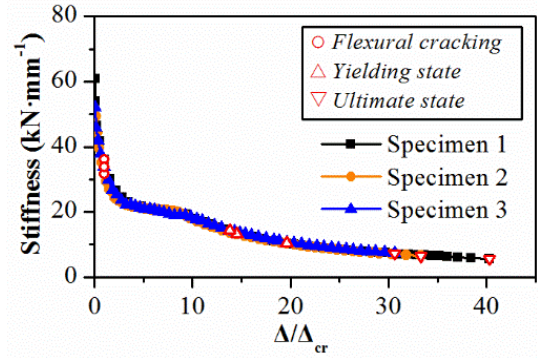


Fig. 8 Stiffness degradation analysis

where Δ_p is the mid-span deflection at peak load; Δ_y is the mid-span deflection at the longitudinal reinforcement yielding; Δ_u is the mid-span deflection at ultimate state.

These two expressions reached a same calculation result in this study because the descending branch of the load-deflection curve was not detected. In order to characterize the post-cracking ductility capacity of the tested specimens, a new ductility index expressed by dividing the ultimate deflection by flexural cracking deflection was introduced

$$\mu_{cr} = \frac{\Delta_u}{\Delta_{cr}} \quad (2)$$

where Δ_{cr} is the mid-span deflection at flexural cracking load.

The calculation result on the ductility indices of the test specimens using equations (1) and (2) is summarized in Table 1. The average values of the ductility indices μ_{cr} and μ_u are 34.7 and 2.2, indicating considerable deformability after cracking and yielding of longitudinal reinforcement.

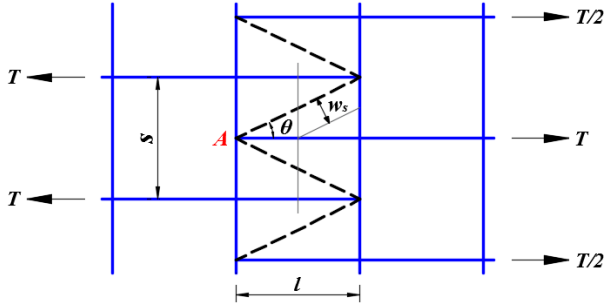
3.4 Stiffness

Fig. 8 illustrates specimen stiffness degradation in which the specimen stiffness versus the ratio of the mid-span deflection Δ at any time to the mid-span flexural cracking deflection Δ_{cr} . The stiffness degradation analysis was conducted based on the secant stiffness. Three stages can be concluded for the stiffness degradation process, namely rapid stiffness degradation before cracking, slow stiffness degradation after cracking and before yielding state, and stiffness stabilization stage. The specimen stiffness experienced a fast reduction before cracking due to continuous micro damage at the tension side. After cracking, the stiffness degradation slowed down owing to the stable crack development and no new crack propagation. At last, the specimen stiffness remained a relative stable value until failure.

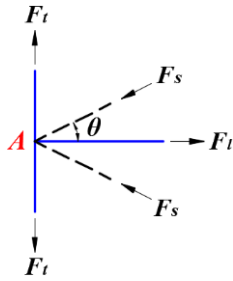
Simultaneously, the flexural performance of the test specimens was evaluated by the relative stiffness degradation at different states, as summarized in Table 2. The parameters k_u , k_y , k_{cr} and k_0 represent the specimen stiffness at ultimate state, longitudinal reinforcement yielding state, flexural cracking state, and initial state, respectively. The specimen stiffness was about 61% of

Table 2 Relative stiffness degradation

| Specimen number | Flexural cracking | | Yielding state | | Ultimate state | |
|-----------------|-------------------|--------------|-------------------|-----------|-------------------|-----------|
| | Δ/Δ_u | k_{cr}/k_0 | Δ/Δ_u | k_y/k_0 | Δ/Δ_u | k_u/k_0 |
| F-1 | 0.02 | 0.59 | 0.49 | 0.17 | 1 | 0.09 |
| F-2 | 0.03 | 0.64 | 0.44 | 0.27 | 1 | 0.13 |
| F-3 | 0.03 | 0.65 | 0.45 | 0.28 | 1 | 0.14 |



(a) STM model



(b) Forces at node A

Fig. 9 STM model for the joint

specimen initial stiffness at flexural cracking while approximate 46% of specimen initial stiffness was reserved at yielding state. At the ultimate state, only 12% of specimen initial stiffness was reserved.

4. Strength prediction of the strut-and-tie model

Due to the discontinuous characteristics of the joint U-bars, their forces must be transferred through the surrounding concrete. The strut-and-tie model (STM) is an efficient method to describe the force transferring path and predict ultimate strength in discontinuity regions of reinforced concrete structures (Schlaich and Schafer 1991). Fig. 9 shows the STM model for the joint in this study. With the help of diagonal concrete compressive struts, the tension forces of U-bars in one side turn back to the other side, thus maintaining continuity of the joint region. Meanwhile, the transverse bars resist the transverse component of the forces in the inclined struts.

Owing to the sufficient anchorage of U-bars, the compression force and the tension force are balanced at the node A. The load capacity of the developed STM model is controlled by the yielding of longitudinal reinforcement, the yielding transverse reinforcement or the crushing of the diagonal concrete strut. Based on force equilibrium condition, the following equations could be obtained

$$F_l = T \quad (3a)$$

$$F_t = T \tan \theta / 2 \quad (3b)$$

$$F_s = T / 2 \cos \theta \quad (3c)$$

where T is the tensile force on the U-bar; F_l , F_s and F_t are the internal forces in the longitudinal bar, transverse bar and concrete strut, respectively. θ is the angle between the longitudinal bar and the concrete strut.

Based on the geometry relationships, the following equations can be obtained

$$\tan \theta = s / 2l \quad (4a)$$

$$\cos \theta = \frac{2l}{\sqrt{4l^2 + s^2}} \quad (4b)$$

$$w_s = l \sin \theta / 2 \quad (4c)$$

where s and l are the spacing and lap length of U-bars; w_s is the width of the inclined compressive strut, which is determined from the diagonal strut width in the truss model for a reinforced concrete beam (Collins and Mitchell 1991). According to ACI 318-14 (ACI Committee 318 2014), the ultimate strength of the concrete diagonal strut is $F_s = 0.85f_c A_s$, in which f_c is the compressive strength of the concrete and A_s is the cross sectional area of a strut. Substituting Eq. (4) into Eq. (3), the load capacity of the proposed STM model controlled by each member is expressed as

$$T_{u,l} = f_{y,l} A_l \quad (5a)$$

$$T_{u,t} = 4f_{y,t} A_t l / s \quad (5b)$$

$$T_{u,s} = \frac{1.7f_c D s l^2}{4l^2 + s^2} \quad (5c)$$

where $f_{y,l}$ and A_l are the yielding strength and area of the longitudinal bars; $f_{y,t}$ and A_t are the yielding strength and area of the transverse bars; D is the bending diameter of U-bars. For a tension joint with a number of N bars on one side, the ultimate capacity can be determined by

$$\begin{aligned} T_u &= N \times \min(T_{u,l}, T_{u,t}, T_{u,s}) \\ &= N \times \min(f_{y,l} A_l, \frac{4f_{y,t} A_t l}{s}, \frac{1.7f_c D s l^2}{4l^2 + s^2}) \end{aligned} \quad (6)$$

Sectional analysis method can be used to estimate the moment capacity of a joint member because the flexure behavior is significant. The ultimate compression force in the top zone is equal to the tension force in the bottom zone. Since the stress limit of $0.85f_c$ is imposed when the failure of the concrete occurs, the ultimate moment capacity of the longitudinal joint can be obtained by

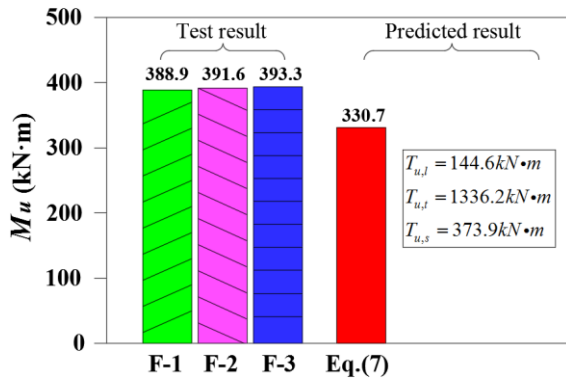


Fig. 10 Comparison between test and prediction results

$$M_u = T_u(d - c/2) \quad (7)$$

where d is the effective depth; c is the depth of the neutral axis and can be calculated by $c = T_u / 0.85f_c b$; b is the width of the specimen.

Fig. 10 shows the predicted $T_{u,l}$, $T_{u,t}$, $T_{u,s}$ and M_u for the test specimens according to Eqs. (3)-(7). The proposed STM model provided a safe prediction of the flexural moment capacity for the test specimens. The under estimation on the flexural strength was attributed to the stress exceeding the yielding strength in the longitudinal reinforcement at ultimate. The calculation results indicate that the ultimate capacity of the joint is controlled by the yielding of the longitudinal reinforcement, which is also confirmed by the test result of large opening of flexural cracks and yielding of the longitudinal reinforcement. It should be noted that the ultimate capacity controlled by concrete diagonal strut is much higher than the ultimate capacity controlled by the yielding of the longitudinal reinforcement or the transverse reinforcement. This result indicates that more reinforcement or higher grade reinforcement should be cooperatively used to take full advantage of the superior mechanical property of UHPC.

5. Conclusions

An experimental test on the flexural behavior of an innovative dovetail UHPC joint of the 5th Nanjing Yangtze River Bridge was conducted using three specimens. The model prototype was chosen from the real bridge and had a dimension of $3600 \times 1600 \times 170$ mm. Based on the analysis of the test results and comparison between STM model and test results, it can be stated that:

- The average nominal flexural cracking strength of the test specimens is 7.7 MPa, signifying good crack resistance of the proposed dovetail UHPC joint. At failure, the ratio of deflection to span is about 1/30, indicating good deformability and ductility.

- Different from conventional reinforced concrete slabs, typical multi-cracking characteristic with small spacing was observed for UHPC joint slabs at failure. Only local layered peeling of compression zone concrete occurred although the concrete compressive strain exceeded the ultimate compressive strain.

- A new ductility index, expressed by dividing the ultimate deflection by flexural cracking deflection, was introduced to characterize the post-cracking ductility capacity. The average values of the ductility indices μ_{cr} and μ_u were 34.7 and 2.2, indicating considerable deformability after cracking and yielding of longitudinal reinforcement.

- It is recommended that high grade reinforcement be cooperatively used to take full advantage of the superior mechanical property of UHPC.

- The proposed STM model provided a safe prediction of the flexural moment capacity for the test UHPC joint specimens with U-bar details.

Acknowledgments

This study was supported by the National Natural Science Foundation of China (Grant No. 51908122, U1934205, 51678140), “Zhishan” Scholars Programs of Southeast University, the Technology R&D Project of China Communications Construction Company (grant number: 2018-ZJKJ-02) and the Fundamental Research Funds for the Central Universities (2242019K40073, 2242019R10). The financial supports are gratefully appreciated.

References

- ACI (American Concrete Institute) (2014), “Building code requirements for structural concrete (ACI 318-14) and commentary.” ACI 318R-14, Farmington Hills, MI, USA.
- Arafa, A., Farghaly, A.S., Ahmed, E.A. and Benmokrane, B. (2016), “Laboratory testing of GFRP-RC panels with UHPFRC joints of the Nipigon River cable-stayed bridge in Northwest Ontario, Canada”, *J. Bridge Eng.*, **21**(11), 05016006. [https://doi.org/10.1061/\(ASCE\)BE.1943-5592.0000943](https://doi.org/10.1061/(ASCE)BE.1943-5592.0000943).
- Bandelt, M.J. and Billington, S.L. (2016), “Bond behavior of steel reinforcement in high-performance fiber-reinforced cementitious composite flexural members”, *Mater. Struct.*, **49**, 71-86. <https://doi.org/10.1617/s11527-014-0475-4>.
- Collins, M.P. and Mitchell, D. (1991), “Prestressed Concrete Structures”, Prentice-Hall, Englewood Cliffs, NJ, USA.
- De la Varga, I., Haber, Z.B. and Graybeal, B.A. (2018), “Enhancing shrinkage properties and bond performance of prefabricated bridge deck connection grouts: Material and component testing”, *J. Mater. Civil Eng.*, **30**(4), 04018053. [https://doi.org/10.1061/\(ASCE\)MT.1943-5533.0002235](https://doi.org/10.1061/(ASCE)MT.1943-5533.0002235).
- Farzad, M., Shafieifar, M. and Azizinamini, A. (2019), “Experimental and numerical study on an innovative sandwich system utilizing UPFRC in bridge applications”, *Eng. Struct.*, **180**, 349-356. <https://doi.org/10.1016/j.engstruct.2018.11.052>.
- GB/T 50081-2002 (2002), “Standard for test method of mechanical properties on ordinary concrete.” Ministry of Construction of the People’s Republic of China, Beijing.
- Grace, N., Ushijima, K., Baah, P. and Beaway, M. (2012), “Flexural behavior of a carbon fiber-reinforced polymer prestressed decked bulb T-beam bridge system”, *J. Compos. Constr.*, **17**(4), 497-506. [https://doi.org/10.1061/\(ASCE\)CC.1943-5614.0000345](https://doi.org/10.1061/(ASCE)CC.1943-5614.0000345).
- Graybeal, B.A. (2008), “Flexural behavior of an ultrahigh-performance concrete I-girder”, *J. Bridge Eng.*, **13**(6), 602-610. [https://doi.org/10.1061/\(ASCE\)1084-0702\(2008\)13:6\(602\)](https://doi.org/10.1061/(ASCE)1084-0702(2008)13:6(602)).
- Graybeal, B.A. (2010), “Behavior of field-cast ultra-high

- performance concrete bridge deck connections under cyclic and static structural loading”, Rep. No. FHWA-HRT-11-023, Federal Highway Administration, McLean, VA, USA.
- Haber, Z.B. and Graybeal, B.A. (2018), “Lap-spliced rebar connections with UHPC closures”, *J. Bridge Eng.*, **23**(6), 04018028. [https://doi.org/10.1061/\(ASCE\)BE.1943-5592.0001239](https://doi.org/10.1061/(ASCE)BE.1943-5592.0001239).
- Le Hoang, A. and Fehling, E. (2017a), “A review and analysis of circular UHPC filled steel tube columns under axial loading”, *Struct. Eng. Mech.*, **61**(2), 417-430. <https://doi.org/10.12989/sem.2017.62.4.417>.
- Le Hoang, A. and Fehling, E. (2017b), “Assessment of stress-strain model for UHPC confined by steel tube stub columns”, *Struct. Eng. Mech.*, **63**(3), 371-384. <https://doi.org/10.12989/sem.2017.63.3.371>.
- Lee, J.K. and Lee, S.H. (2015), “Flexural behavior of ultra-high-performance fiber-reinforced concrete moment connection for precast concrete decks”, *ACI Struct. J.*, **112**(4), 451-462. <https://doi.org/10.14359/51687657>.
- Mirmiran, A. Sadaghian, H. and Pourbaba, M. (2019), “Flexural response of UHPFRC beams reinforced with steel rebars”, *Adv. Civil Eng. Mater.*, **8**(3), 411-430. <https://doi.org/10.1520/ACEM20190129>.
- Nguyen, C.V., Le, A.H. and Thai, D.K. (2019), “Numerical simulation and analytical assessment of STCC columns filled with UHPC and UHPFRC”, *Struct. Eng. Mech.*, **70**(1), 13-31. <https://doi.org/10.12989/sem.2019.70.1.013>.
- Parra-Montesinos, G.J. (2005), “High-performance fiber-reinforced cement composites: an alternative for seismic design of structures”, *ACI Struct. J.*, **102**(5), 668-675.
- Pourbaba, M. Asefi, E. Sadaghian, H. and Mirmiran, A. (2018), “Effect of age on the compressive strength of ultra-high-performance fiber-reinforced concrete”, *Constr. Build. Mater.*, **175**, 402-410. <https://doi.org/10.1016/j.conbuildmat.2018.04.203>.
- Pourbaba, M. Sadaghian, H. and Mirmiran, A. (2019), “A comparative study of flexural and shear behavior of ultra-high-performance fiber-reinforced concrete beams”, *Adv. Struct. Eng.*, **22**(7), 1727-1738. <https://doi.org/10.1177/1369433218823848>.
- Qi, J., Ma, Z.J., Wang, J. and Liu, T. (2016), “Post-cracking shear strength and deformability of HSS-UHPFRC beams”, *Struct. Concr.*, **17**(6), 1033-1046. <https://doi.org/10.1002/suco.201500191>.
- Qi, J., Bao, Y., Wang, J., Li, L., and Li, W. (2019a), “Flexural behavior of an innovative dovetail UHPC joint in composite bridges under negative bending moment”, *Eng. Struct.*, **200**, 109716. <https://doi.org/10.1016/j.engstruct.2019.109716>.
- Qi, J., Ding, X., Wang, Z. and Hu, Y. (2019b), “Shear strength of fiber-reinforced HSS-UHPC beams based on refined calculation of compression zone depth considering concrete tension”, *Adv. Struct. Eng.*, **22**(8), 2006-2018. <https://doi.org/10.1177/1369433219829805>.
- Qi, J., Ma, Z.J. and Wang, J. (2017), “Shear strength of UHPFRC beams: mesoscale fiber-matrix discrete model”, *J. Struct. Eng.*, **143**(4), 04016209. [https://doi.org/10.1061/\(ASCE\)ST.1943-541X.0001701](https://doi.org/10.1061/(ASCE)ST.1943-541X.0001701).
- Qi, J., Wang, J. and Feng, Y. (2019), “Shear performance of an innovative UHPFRC deck of composite bridge with coarse aggregate”, *Adv. Concr. Constr.*, **7**(4): 219-229. <https://doi.org/10.12989/acc.2019.7.4.219>.
- Qi, J., Wang, J. and Ma, Z.J. (2018b), “Flexural response of high-strength steel-ultra-high-performance fiber reinforced concrete beams based on a mesoscale constitutive model: Experiment and theory”, *Struct. Concr.*, **19**(3), 719-734. <https://doi.org/10.1002/suco.201700043>.
- Qi, J., Wu, Z., Ma, Z.J. and Wang, J. (2018a), “Pullout behavior of straight and hooked-end steel fibers in UHPC matrix with various embedded angles”, *Constr. Build. Mater.*, **191**, 764-774. <https://doi.org/10.1016/j.conbuildmat.2018.10.067>.
- Russell, H.G. Graybeal, B.A. and Russell, H.G. (2013), “Ultra-high performance concrete: a state-of-the-art report for the bridge community (No. FHWA-HRT-13-060)”, United States. Federal Highway Administration. Office of Infrastructure Research and Development.
- Saleem, M.A. Mirmiran, A. Xia, J. and Mackie, K. (2011), “Ultra-high-performance concrete bridge deck reinforced with high-strength steel”, *ACI Struct. J.*, **108**(5), 601-609.
- Saleem, M.A. Mirmiran, A. Xia, J. and Mackie, K. (2012), “Development length of high-strength steel rebar in ultrahigh performance concrete”, *J. Mater. Civil Eng.*, **25**(8), 991-998. [https://doi.org/10.1061/\(ASCE\)MT.1943-5533.0000571](https://doi.org/10.1061/(ASCE)MT.1943-5533.0000571).
- Schlaich, J. and Schafer, K. (1991), “Design and detailing of structural concrete using strut-and-tie models”, *Struct. Eng.*, **69**(6), 113-125.
- Vergier-Leboeuf, S., Charron, J.P. and Massicotte, B. (2017), “Design and behavior of UHPFRC field-cast transverse connections between precast bridge deck elements”, *J. Bridge Eng.*, **22**(7), 04017031. [https://doi.org/10.1061/\(ASCE\)BE.1943-5592.0001064](https://doi.org/10.1061/(ASCE)BE.1943-5592.0001064).
- Wang, J., Qi, J., Tong, T., Xu, Q. and Xiu, H. (2019), “Static behavior of large stud shear connectors in steel-UHPC composite structures”, *Eng. Struct.*, **178**, 534-542. <https://doi.org/10.1016/j.engstruct.2018.07.058>.
- Yoo, D.Y. and Yoon, Y.S. (2015), “Structural performance of ultra-high-performance concrete beams with different steel fibers”, *Eng. Struct.*, **102**, 409-423. <https://doi.org/10.1016/j.engstruct.2015.08.029>.
- Zhou, M. Lu, W. Song, J. and Lee, G.C. (2018), “Application of ultra-high performance concrete in bridge engineering”, *Constr. Build. Mater.*, **186**, 1256-1267. <https://doi.org/10.1016/j.conbuildmat.2018.08.036>.

CC